Strength analysis of composite cables

Abstract

Carbon Fiber Reinforced Polymer (CFRP) cables, due to their outstanding performance in terms of specific stiffness and strength, are usually found in civil construction applications and, more recently, in the Oil & Gas sector. However, experimental data and theoretical solutions for these cables are very limited. On the contrary, several theoretical and numerical approaches are available for isotropic cables (metallic wire ropes), some of them with severe simplifications, nonetheless showing good agreement with experimental data. In this study, experimental tensile results for 1×7 CRFP cables were compared to a simplified analytical model (assumed transversally isotropic) and to a 3D finite element model incorporating the experimental uncertainty in important input parameters: longitudinal elastic modulus, Poisson's ratio, static friction coefficient and ultimate tensile strain. The average experimental breaking load of the cable was 190.25 kN (coefficient of variation of 1.74%) and the agreement with the numerical model predictions were good, with an average-value deviation of −1.15%, which is lower than the experimental variations. The simplified analytical model yielded a discrepancy above 10%, indicating that it needs further refinement although much less time consuming than the numerical model. These conclusions were corroborated by statistical analyses (i.e. Kruskal–Wallis and Mann-Whitney).

Keywords

Composite cables, finite element analysis, analytical model, design of experiments, uncertainty quantification.

Felipe Ferreira Luz [a]*
Eduardo Antonio Wink de Menezes [a]
Laís Vasconcelos da Silva [a]
Carlos Alberto Cimini Jr.[b]
Sandro Campos Amico [a]

[a] Departamento de Engenharia de Materiais, Universidade Federal do Rio Grande do Sul, Porto Alegre, RS, Brazil. Email: felipe.ferreira.luz@gmail.com, eduardo.menezes@ufrgs.br, laisvasc@gmail.com, amico@ufrgs.br.

[b] Departamento de Engenharia de Estruturas, Universidade Federal de Minas Gerais, Belo Horizonte, MG, Brazil. Email: cimini@ufmg.br.

*Corresponding author

http://dx.doi.org/10.1590/1679-78254177

1 INTRODUCTION

Carbon Fiber Reinforced Polymer (CFRP) cables present high stiffness-to-weight and strength-to-weight ratios, damping capabilities and high resistance to environmental degradation (Adanur et al., 2015), being natural candidates for harsh environments such as offshore applications. While the cost of composite materials is generally greater than that of traditional structural materials, their extended life leads to reduced long-term costs (Fabbrocino et al., 2016). Other benefits include low energy consumption during manufacturing, construction and execution processes (Dhand et al., 2015; Son et al, 2013; Wang and Wang, 2015).

CFRP cables are traditionally manufactured by pultrusion using epoxy resin, allowing the use of long fibers and high fiber volume fraction. According to Meier (2012), Meier et al. (1982), Meier (1992) and Rohleder et al. (2008), in order to encourage the use of composite cables in structural applications, it is necessary to fully study and understand their behavior, which could be translated as evaluating analytical solutions, constructing numerical models and executing experimental tests. Indeed, there is very limited experimental data in the literature for these cables and theoretical solutions still require further development.

On the contrary, several theoretical approaches have been developed for isotropic cables (metallic wire ropes), some of them with severe simplifications, nonetheless showing good agreement with experimental data. Costello (1997) extensively investigated isotropic cables developing analytical models based on beam theory. Unlike most of the previous analytical solutions, he treated the wires as rods, allowing bending and torsion stiffness analysis. Usabiaga and Pagalday (2008), also using beam theory, developed an analytical solution for isotropic cables submitted to tensile stress considering rod rotation, but neglected the Poisson's effect, and verified a small difference with the results of Costello (1997) for Poisson's ratio of 0.0 and 0.3.

On the numerical field, Erdonmez and Imrak (2011) analyzed 6×7 Stranded isotropic cables using the FEM (finite element method). They investigated the minimum length to be modeled that could still give reliable results, saving computational time and allowing effective contact between wires. They concluded that wire contraction

played a small role on the mechanical behavior. Jiang (2012) analyzed isotropic single-layered strand cables in pure bending considering plastic strain and friction and also achieved good agreement with Costello (1997) analytical solution. Ghoreishi et al. (2007) compared their FEM model results with experimental data for a 1×7 single-layered isotropic cable under axial loading, varying helix angle, and obtained small variations. They also analyzed the same cable using nine different analytical models, including Costello (1997), with different considerations and assumptions, and reported satisfactory estimations of the elastic stiffness constants for lay angles below 20°.

Composite cables have been scarcely used in the petroleum sector. Jackson et al. (2005) used a spiral Carbon Fiber Composite Cable (CFCC) and ran tensile and cyclic fatigue tests with satisfactory results. However, they reported issues with the manufacturing process and no analytical or numerical model was used. Sparks et al. (2003) studied CFCC in the offshore industry, more specifically in TLP (tension leg platforms) used in ultra-deep waters, and reported advantages as: good fatigue resistance, high level of flexibility, safety due to the non-propagation of defects, and unlimited size for mooring.

Even if a state-of-the-art numerical model was available, the predictions could differ from experimental results as they, unlike the latter, do not include statistical variations (Grover et al., 2017). And since quality of composite materials is severely influenced by the quality control of processes, operating conditions and environmental effects, uncertainties in input parameters can propagate through different modelling scales and significantly influence other parameters and the final output due to risk accumulation (Shaw et al., 2010).

To allow associating experimental design to a virtual model simulation, the methodology of Design of Experiments (DEX) was applied in the analysis of tensile strength of a commercial 1×7 CFRP composite cable to account for uncertainties (Fong et al., 2013). More specifically, the study focused on how carbon fiber composite cables responses in terms of tensile load and on the sensitivity analysis of the strength estimate to four main design parameters, ultimate tensile strain of the rod, longitudinal elastic modulus, Poisson's ratio and the static friction coefficient between rods/wires. This work is organized as follows, (ii) Experiments shows how the rods and cables were tested for ultimate tensile strain, longitudinal elastic modulus, Poisson's ratio and static friction, (ii) Simplified Analytical Model for Transversely Isotropic Material presents the equations used to describe the cable's behavior, (iii) Finite Element Model exhibits the numerical method and its boundary conditions, (iv) Results shows and analyzes the experimental data and its correlation with the models, and (v) our conclusions.

2 EXPERIMENTS

Standard 1×7 commercial CFRP cable was selected for this study. This cable is composed of six outer wires (3.5 mm diameter) helically twisted around a core of the same diameter. Nominal diameter of the cable is 10.5 mm and pitch length is 152 mm. Fiber volume fraction of the rods was experimentally determined according to the ASTM D3171 as 68%.

Tensile tests of the cables were performed according to the Japanese Standard JSCE-E 531 (1995) using a 170-ton horizontal testing machine (Figure 1a). The length of the anchor region at the cable ends, which was socketed with expansive cement, was 330 mm, and the central gauge region was 3360 mm long, as shown in Figure 1b.

Strain data was not collected in this test because it was not possible to attach strain gauges to the core rod of the cable which was closely surrounded by six other rods. Instead, a similar test program was performed for single straight CFRP rods (the core rod) to calculate ultimate tensile strain (ε_{1t}^u), longitudinal elastic modulus (E_1) and Poisson's ratio (ν_{12}). For this cable architecture, strain is maximum at its core, which is straight and takes more load (Costello, 1997; Erdonmez and Imrak, 2011). Using ASTM-D3916, four samples were instrumented with strain gauges and tested in Instron universal testing machine.

From these measurements, it was possible to use the invariant-based method proposed by Tsai and Melo (2014), which introduced the master-ply concept (same trace-normalized unidirectional lamina stiffness properties). This is expected to yield good results for thermoset resins reinforced with high volume fraction of carbon fibers, which is adequate for the CFRP analyzed in this study.

The Static Friction Coefficient (SFC) used as input in the numerical modelling was obtained using a dedicated equipment for static friction analysis. Since the contact area between two cylindrical rods is small and variable, which can lead to scattered results, the rods were cut longitudinally, producing two halves, and one of them received an extra cut to produce a flat bottom surface to allow fixing to the equipment. The top half was positioned over the bottom half as shown in Figure 2 and their position was monitored with laser sensor, which detects when the top half starts to slide over the fixed bottom half. Ten pairs of samples (top and bottom) were tested with 5 SFC measurements for each pair.
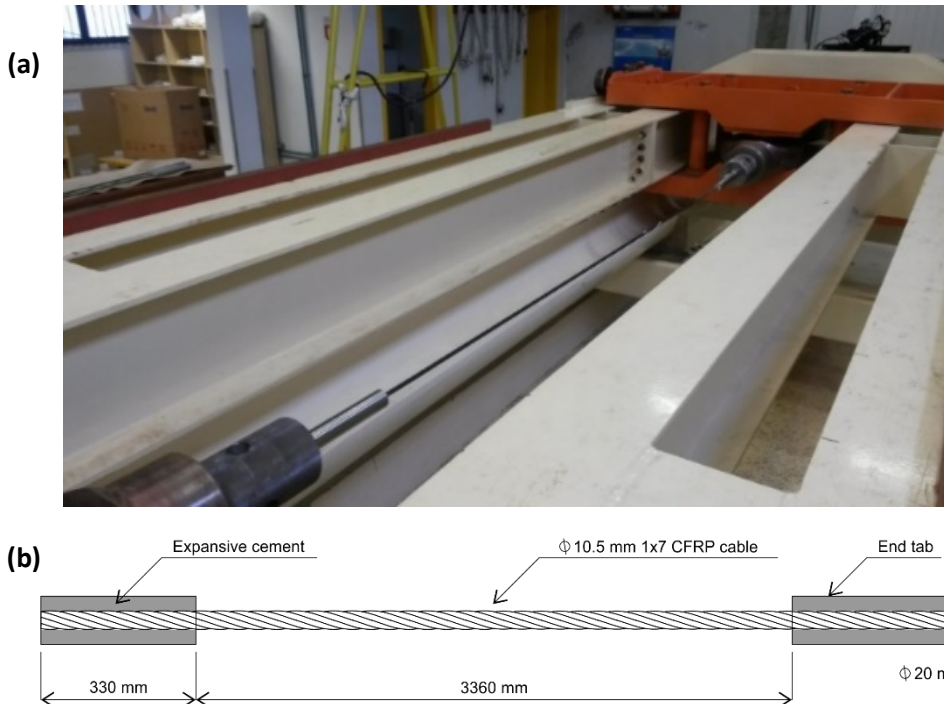
Figure 1: (a) CFRP cable attached to the tensile testing equipment, (b) detailing of the cable geometry and socketing scheme.
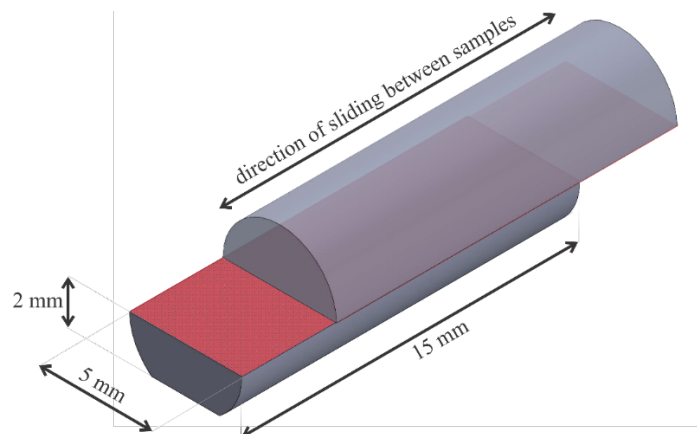
Figure 2: Rod halves assembly and dimensions for the SFC tests.

3 SIMPLIFIED ANALYTICAL MODEL FOR TRANSVERSELY ISOTROPIC MATERIAL

The analytical model used in this study is a simplified model based on Costello (1997), adapted for a transversely isotropic material. Since the rods used in the CFRP cables were produced by pultrusion, where all the fibers are aligned in the same direction and homogeneously distributed within a circular cross-section, the transversely isotropic symmetry was chosen to describe them.

The 1×7 cable is the sub-element of more complex wire ropes. Therefore, this model consists in the use of kinematics of a thin wire to get the equilibrium equations. The full based analytical model, with all the assumptions, limitations and original equations can be found in Costello (1997). Figure 3 shows the loads acting on the cable (a) and on a single helical rod (b), and Equations (1)-(8) describe the static response of a 1×7 stranded cable, which, in this study, differs from the original Costello (1997) due to anisotropic material assumptions: E_1 is used instead of E, ν_{12} is used instead of ν and the lay angle is considered for fiber alignment in the outside wires.

$$\frac{G_{2,ow}}{(E_1 sen\,\alpha)R_{ow}^3} = \frac{\pi}{4}R_{ow}\Delta\kappa_{2,ow} \tag{1}$$

$$\frac{H_{ow}}{(E_1 sen\,\alpha)R_{ow}^3} = \frac{\pi}{4(1+\nu_{12})}R_{ow}\Delta\tau_{ow} \tag{2}$$

$$\frac{N_{2,ow}}{(E_1 sen\,\alpha)R_{ow}^2} = \frac{H_{ow}}{(E_1 sen\,\alpha)R_{ow}^3}\frac{\cos^2\alpha}{r_{ow}\big/R_{ow}} - \frac{G_{2,ow}}{(E_1 sen\,\alpha)R_{ow}^3}\frac{sen\,\alpha\cos\alpha}{r_{SW}\big/R_{SW}} \tag{3}$$

$$\frac{T_{ow}}{(E_1 sen\,\alpha)R_{ow}^2} = \pi\xi_{ow} \tag{4}$$

$$\frac{X_{ow}}{(E_1 sen\,\alpha)R_{ow}} = \frac{N_{2,ow}}{(E_1 sen\,\alpha)R_{ow}^2}\frac{sen\,\alpha\cos\alpha}{r_{ow}\big/R_{ow}} - \frac{T_{ow}}{(E_1 sen\,\alpha)R_{ow}^3}\frac{\cos^2\alpha}{r_{ow}\big/R_{ow}} \tag{5}$$

$$\frac{F_{ow}}{(E_1 sen\,\alpha)R_{ow}^2} = m_{ow}\left[\frac{T_{ow}}{(E_1 sen\,\alpha)R_{ow}^2}sen\,\alpha + \frac{N_{2,ow}}{(E_1 sen\,\alpha)R_{ow}^2}\cos\alpha\right] \tag{6}$$

$$\frac{F_C}{(E_1)R_C^2} = \pi\xi_C \tag{7}$$

$$F = F_C + F_{ow} \tag{8}$$

where α is the helix (lay) angle; N is the shearing force on a wire cross section; τ is the twist per unit length; T is the axial tension in the wire; X is the component of the external line load per unit length of the centerline of the wire in the 1 direction; k is the curvature; G is the bending moment on a wire cross-section; H is the twisting moment in the wire; K is the external moment per unit length of the centerline; F is the total axial force; $r = R_c + R_{ow}$. The subscripts 1, 2 and 3 refer to the components in the 1, 2 and 3 directions, respectively, while c and ow refer to core and outside wires, respectively.
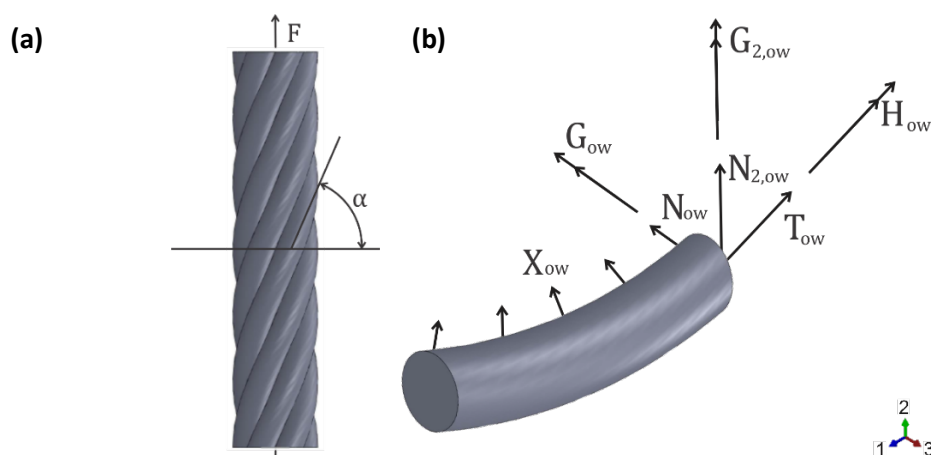
Figure 3: Loads acting on the 1×7 CFRP cable (a) and on a single helical rod (b).

4 FINITE ELEMENT MODEL

The numerical finite element model was developed within the commercial finite element platform Abaqus™ using a tetrahedral mesh with ten-node linear brick elements and three degrees of freedom per node (C3D10 in

Abaqus™ mesh library) as seen in Figure 4a. The 1×7 Stranded cable geometry was modeled using 10,533 nodes and 32,075 elements. The orthotropic material of each wire in the strand was oriented with its fiber axis set along the helix axis, as seen in Figure 4b. Surface-to-surface contact type was defined between surfaces of adjacent wires of the strand, 12 pairs in total, and one of them is highlighted in Figure 4c. Friction was taken into account in the contact based on the static friction coefficient. Boundary conditions considered built-in restrictions in both cable ends, but allowing torsion rotation along the longitudinal (z) axis at one end. Pure tensile stress loading was applied and maximum strain failure criterion was considered in all numerical simulations, using ε_{1t}^{u} as failure parameter.
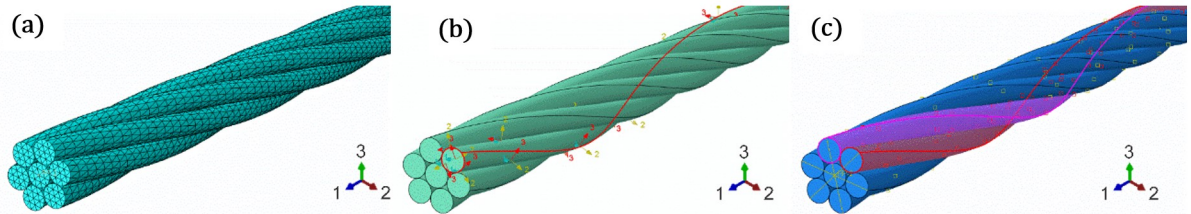
Figure 4: *3D numerical finite element model of the CFRP cable: (a) mesh with 8-node tetrahedral elements, (b) description of material orientation (fiber axis) along the helix length and (c) highlighting of one of the 12 contact pairs.*

5 RESULTS

Table 1 presents the tensile breaking loads of four 1×7 CFRP cable specimens (mean value of 190.25 kN). Table 1 also shows the results from single straight CFRP rods, with mean longitudinal elastic modulus, major Poisson's ratio and ultimate tensile strain of 141.6 GPa, 0.28 and 1.64%, respectively. From the friction tests, the mean SFC was 0.61. These results for longitudinal elastic modulus, Poisson's ratio and ultimate tensile strain for the single rod are in agreement with others studies using similar rods for cable structures (Adanur et al., 2015; Meier, 2012; Cai and Aref, 2015; Wang and Wu, 2010; Schmidt et al., 2010). Table 2 shows the material properties estimated based on Tsai-Melo method for master-ply, these values are congruent with the available data for carbon / epoxy composites, which also can be seen in Tsai and Melo (2014).

Table 1: *Experimental results for CFRP cable and single straight CFRP rod.*

	1×7 CFRP cable	Single CFRP rod			
	Breaking load (kN)	E_1 (GPa)	ν_{12}	SFC	ε_{1t}^{u}
Average	190.25	141.60	0.28	0.61	1.64%
σ	3.31	6.01	0.02	0.05	0.15
CV	1.74%	4.24%	7.14%	8.20%	9.15%

Table 2: *CFRP rod elastic properties estimated using Tsai and Melo (2014) trace invariant method.*

$E_1 = 141.6$ GPa (± 6)*	$G_{12} = 5.3$ GPa	$\nu_{12} = 0.28$ (± 0.02)*
$E_2 = 7.6$ GPa	$G_{13} = 5.3$ GPa	$\nu_{13} = 0.28$
$E_3 = 7.6$ GPa	$G_{23} = 4.7$ GPa	$\nu_{23} = 0.47$

* Experimentally measured.

In order to insert probabilistic uncertainties into the simulations, both models incorporated variations in the main input properties. Uncertainty was represented by one standard deviation ($\pm \sigma$) in: longitudinal elastic modulus, Poisson's ratio, and SFC. Maximum tensile strain was adopted as failure criteria, which means that each simulation generated three different breaking loads considering the uncertainty of the ultimate failure strain ($\overline{\varepsilon}_{1t}^{-u}$, $\overline{\varepsilon}_{1t}^{-u-\sigma}$ and $\overline{\varepsilon}_{1t}^{-u+\sigma}$). Therefore, the numerical model produced a total of 81 strength results, and the simplified analytical solution, 27 strength results (it did not include friction), as shown in Table 3.

Table 3: *Breaking load (kN) simulation results for each model.*

Model			$\varepsilon_{1t}^{-u-\sigma}$ Numerical	Analytical	ε_{1t}^{-u} Numerical	Analytical	$\varepsilon_{1t}^{-u+\sigma}$ Numerical	Analytical
Run-1	$\overline{E_1}^{-\sigma}$	$\overline{\nu_{12}}^{-\sigma}$ $\overline{SFC}^{-\sigma}$	164.27		180.81		197.34	
Run-2	$\overline{E_1}^{-\sigma}$	$\overline{\nu_{12}}^{-\sigma}$ $\overline{SFC}$	164.39	184.64	180.94	203.23	197.49	221.82
Run-3	$\overline{E_1}^{-\sigma}$	$\overline{\nu_{12}}^{-\sigma}$ $\overline{SFC}^{+\sigma}$	164.46		181.01		197.57	
Run-4	$\overline{E_1}^{-\sigma}$	$\overline{\nu_{12}}$ $\overline{SFC}^{-\sigma}$	164.08		180.60		197.12	
Run-5	$\overline{E_1}^{-\sigma}$	$\overline{\nu_{12}}$ $\overline{SFC}$	164.21	184.55	180.74	203.13	197.27	221.71
Run-6	$\overline{E_1}^{-\sigma}$	$\overline{\nu_{12}}$ $\overline{SFC}^{+\sigma}$	164.27		180.81		197.34	
Run-7	$\overline{E_1}^{-\sigma}$	$\overline{\nu_{12}}^{+\sigma}$ $\overline{SFC}^{-\sigma}$	163.83		180.33		196.82	
Run-8	$\overline{E_1}^{-\sigma}$	$\overline{\nu_{12}}^{+\sigma}$ $\overline{SFC}$	163.96	184.46	180.46	203.03	196.97	221.59
Run-9	$\overline{E_1}^{-\sigma}$	$\overline{\nu_{12}}^{+\sigma}$ $\overline{SFC}^{+\sigma}$	164.08		180.60		197.12	
Run-10	$\overline{E_1}$	$\overline{\nu_{12}}^{-\sigma}$ $\overline{SFC}^{-\sigma}$	171.05		188.27		205.49	
Run-11	$\overline{E_1}$	$\overline{\nu_{12}}^{-\sigma}$ $\overline{SFC}$	171.12	192.81	188.35	212.22	205.57	231.63
Run-12	$\overline{E_1}$	$\overline{\nu_{12}}^{-\sigma}$ $\overline{SFC}^{+\sigma}$	171.19		188.42		205.65	
Run-13	$\overline{E_1}$	$\overline{\nu_{12}}$ $\overline{SFC}^{-\sigma}$	170.78		187.97		205.17	
Run-14	$\overline{E_1}$	$\overline{\nu_{12}}$ $\overline{SFC}$	170.92	192.71	188.12	212.12	205.33	231.52
Run-15	$\overline{E_1}$	$\overline{\nu_{12}}$ $\overline{SFC}^{+\sigma}$	170.98		188.20		205.41	
Run-16	$\overline{E_1}$	$\overline{\nu_{12}}^{+\sigma}$ $\overline{SFC}^{-\sigma}$	170.58		187.75		204.92	
Run-17	$\overline{E_1}$	$\overline{\nu_{12}}^{+\sigma}$ $\overline{SFC}$	170.64	192.62	187.82	212.01	205.00	231.40
Run-18	$\overline{E_1}$	$\overline{\nu_{12}}^{+\sigma}$ $\overline{SFC}^{+\sigma}$	170.78		187.97		205.17	
Run-19	$\overline{E_1}^{+\sigma}$	$\overline{\nu_{12}}^{-\sigma}$ $\overline{SFC}^{-\sigma}$	177.68		195.57		213.46	
Run-20	$\overline{E_1}^{+\sigma}$	$\overline{\nu_{12}}^{-\sigma}$ $\overline{SFC}$	177.76	200.98	195.65	221.22	213.54	241.45
Run-21	$\overline{E_1}^{+\sigma}$	$\overline{\nu_{12}}^{-\sigma}$ $\overline{SFC}^{+\sigma}$	177.90		195.81		213.72	
Run-22	$\overline{E_1}^{+\sigma}$	$\overline{\nu_{12}}$ $\overline{SFC}^{-\sigma}$	177.46		195.33		213.19	
Run-23	$\overline{E_1}^{+\sigma}$	$\overline{\nu_{12}}$ $\overline{SFC}$	177.61	200.88	195.49	221.10	213.37	241.33
Run-24	$\overline{E_1}^{+\sigma}$	$\overline{\nu_{12}}$ $\overline{SFC}^{+\sigma}$	177.68		195.57		213.46	
Run-25	$\overline{E_1}^{+\sigma}$	$\overline{\nu_{12}}^{+\sigma}$ $\overline{SFC}^{-\sigma}$	177.24		195.09		212.93	
Run-26	$\overline{E_1}^{+\sigma}$	$\overline{\nu_{12}}^{+\sigma}$ $\overline{SFC}$	177.39	200.78	195.25	220.99	213.11	241.20
Run-27	$\overline{E_1}^{+\sigma}$	$\overline{\nu_{12}}^{+\sigma}$ $\overline{SFC}^{+\sigma}$	177.46		195.33		213.19	

Considering the full population for each approach, the numerical model presented an average load break of 188.1 kN (σ of 15.39 and CV of 8.18%), with an average-value difference of –1.15% compared to experimental results. The average-value difference for the simplified analytical model is 10.31%, with an average breaking load of 212.12 kN (σ of 17.80 and CV 8.38%). Figure 5 displays these results.

The smaller difference presented by the numerical model can be justified by its higher complexity, since it considers a 3D geometry, friction and nine elastic constants. Results from the analytical model indicates that it needs refinement, nonetheless, the numerical model is much more time-intensive than the analytical model.
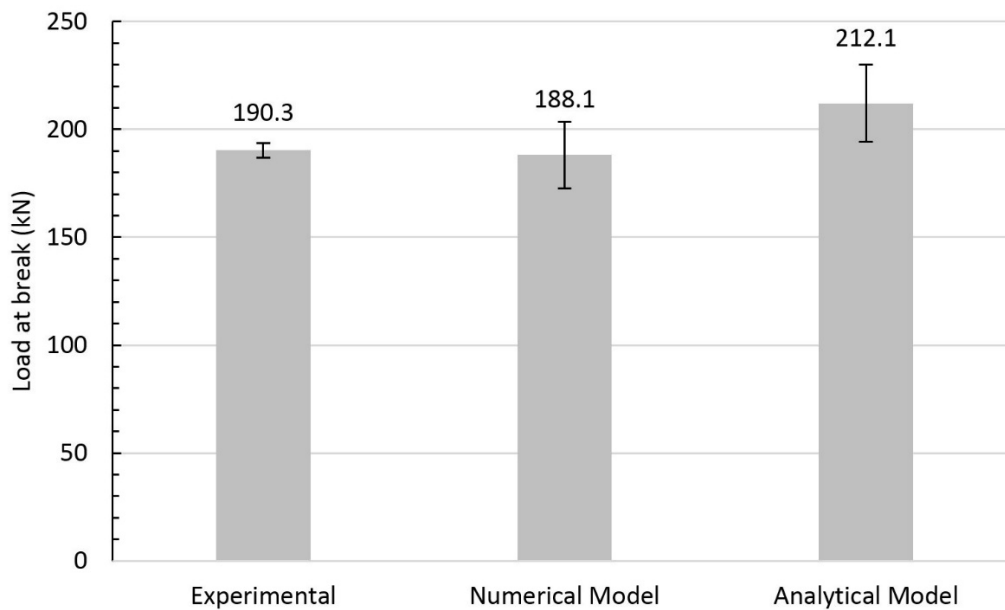
Figure 5: *Breaking load results for experimental, analytical and numerical approaches.*

As for the statistical analysis, a Kolmogorov–Smirnov test was applied in order to check the hypothesis of normality. Levene's test was also applied to check the hypothesis of homogeneity of variance. The p-value from both tests was less than 0.05 (Table 4), indicating that: (i) the data set is non-parametric and (ii) there is no equality of variances in at least one group. Therefore, only non-parametric tests were applied so forth.

In order to check for statistically significant differences between results, a Kruskal–Wallis H test was applied. The p-value was less than 0.05 indicating that there is significant difference between at least one model compared to the experimental results. To find out which group is different, a Mann-Whitney U test was used, and the results can be seen in Table 4. This analysis indicates that there is no significant difference between experimental and numerical results (p-value of 0.852). However, significant difference was found for the analytical model (p-value 0.022). That is, the numerical result was similar to the experiment, but they both differed from the analytical model.

Lastly, in order to verify sensitivity of both models to individual parameters, another Kruskal–Wallis H test was applied. The numerical data was organized into three groups: (i) Runs 5, 14 and 23, (ii) Runs 11, 14 and 17, and (iii) Runs 13, 14 and 15; and the analytical data into two groups: (i) Runs 4-6, 13-15 and 22-24, and (ii) Runs 10-12, 13-15 and 16-18. The results indicate that are no difference between the groups for both models (p-value 1.00 for both analyses). That is, the individual parameters give similar contribution to the model's results.

Table 4: *Statistical analysis for differences between results and sensitivity of both models to individual parameters.*

	Kolmogorov–Smirnov	Levene	Kruskal–Wallis (for differences between models)	Mann-Whitney	Kruskal–Wallis (for individual parameters)
Experimental				-	-
Numerical	< 0.001	0.017	< 0.001	0.852	1.00
Analytical				0.022	1.00

6 CONCLUSIONS

CFRP cables have a great potential to be use in high performance applications for different engineering fields. Experimental tensile testing was conducted in 1×7 CFRP cable specimens resulting in average breaking load of 190.25 kN (σ of 3.31 kN and CV of 1.74%). Simplified analytical and more comprehensive finite element numerical models were developed to estimate cable strength, and probabilistic uncertainties were inserted for both models. The numerical model correlated well with the experimental data, presenting an average-value difference of –1.15%. On the other hand, the analytical model presented an average-value difference above 10%, indicating that it needs refinement, nonetheless being much less time consuming than the numerical model. Statistical analyses indicated high evidence that the numerical result is equal to the experimental one, but not the analytical result. Moreover, the

results from both models are not sensitive to the individual parameters investigated (ultimate tensile strain of the rod, longitudinal elastic modulus, Poisson's ratio and static friction coefficient between rods/wires), and all inputs carried similar contribution to the results.

Acknowledgments

References

Adanur, S., Mosallam, A.S., Shinozuka, M., Gumusel, L., (2015). A comparative study on static and dynamic responses of FRP composite and steel suspension bridges. Journal of Reinforced Plastics and Composites 30(15):1265-1279.

Cai, H., Aref, A.J., (2015). On The Design And Optimization Of Hybrid Carbon Fiber Reinforced Polymer-Steel Cable System For Cable-Stayed Bridges. Composites: Part B 68:146-152.

Costello, G.A., (1997). Theory of Wire Rope. Mechanical Engineering Series, Springer-Verlag, New York.

Dhand, V., Mittal, G., Rhee, K.Y., Park, S.J., Hui, D., (2015). A short review on basalt fiber reinforced polymer composites. Compos. Part B-Eng. 73:166-180.

Erdonmez, C., Imrak, C., (2011). A finite element model for independent wire rope core with double helical geometry subjected to axial loads. Sadhana 36(6):995-1008.

Fabbrocino, F., Modano, M., Farina, I., Carpentieri, G., Fraternali, F., (2016). Optimal prestress design of composite cable-stayed bridges. Compos. Struct. 169:167-172.

Fong, J.T., Cimini, C.A., Melo, J.D.D., Heckert, N.A., Filliben, J.J., (2013). Theoretical Failure Envelopes Of Open Hole Composite Laminates With A- And B-Basis Allowables Estimated From Smooth Specimen Properties. In: 19th International Conference On Composite Materials (ICCM19), Montréal, Canada, pp. 1-11.

Ghoreishi, S.R., Messager, T., Cartraud, P., Davies, P., (2007). Validity and limitations of linear analytical models for steel wire strands under axial loading, using a 3D FE model. International Journal of Mechanical Sciences 49(11):1251-1261.

Grover, N., Sahoo, R., Singh, B.N., Maiti, D.K., (2017). Influence of Parametric Uncertainties on the Deflection Statistics of General Laminated Composite and Sandwich Plates. Composite Structures, doi: http://dx.doi.org/10.1016/j.compstruct.2017.03.036.

Jackson, D., Shepheard, B., Kebadze, E., Teles, R., Rossi, R., Gonçalves, R.C., (2005). CFRP Mooring lines for MODU applications. In: Offshore Technology Conference, Houston, United States, pp. 1-6.

Jiang, W.G., (2012). A concise finite element model for pure bending analysis of simple wire strand. International Journal of Mechanical Sciences 54(1):69-73.

JSCE-E 531 (1995). Test Method for Tensile Properties of Continuous Fiber Reinforcing Materials. Japan Society of Civil Engineers, Tokyo, Japan.

Meier, U., (2012). Carbon Fiber Reinforced Polymer Cables: Why? Why Not? What If? Arabian Journal for Science and Engineering 37:399-411.

Meier, U., (1992). Carbon Fiber Reinforced Polymers: Modern Materials in Bridge Engineering. Structural Engineering International 2(1):7-12.

Meier, U., Müller, R., Puck, A., (1982). GFK-Biegeträger Unter Quasistatischer und Schwingender Beanspruchung. Proceedings of Internationale Tagung Über Verstärkte Kunststoffe, 35:1-35.

Rohleder Jr., W.J., Tang, B., Doe, T.A., Grace, N.F., Burgess, C.J., (2008). CFRP Strand Application on Penobscot Narrows Cable Stayed Bridge. Transportation Research Board Journal 2050:169-176.

Schmidt, J.W., Bennitz, A., Täljsten, B., Pedersen, H., (2010). Development of Mechanical Anchor for CFRP Tendons Using Integrated Sleeve. Journal of Composites for Construction 14:397-405.

Shaw, A., Sriramula, S., Gosling, P.D., Chryssanthopoulos, M.K., (2010). A critical reliability evaluation of fibre reinforced composite materials based on probabilistic micro and macro-mechanical analysis. Composites Part B: Engineering 41(6):446-453.

Sparks, C., Zivanovic, I., Luyckx, J., Hudson, W., (2003). Carbon Fiber Composite Tendons for Deepwater Tension Leg Platforms. In: Offshore Technology Conference, Houston, United States, pp. 1-5.

Son, B.J., Lee, S.Y., Ji, H.S., (2013). Long-term performance of a fiber-reinforced polymer slab bridge superstructure-field load test and ratings. Compos. Part B-Eng. 45(1):644-656.

Tsai, S., Melo, J., (2014). An invariant-based theory of composites. Composites Science and Technology 100:237-243.

Usabiaga, H., Pagalday, J.M., (2008). Analytical procedure for modelling recursively and wire by wire stranded ropes subjected to traction and torsion loads. International Journal of Solids and Structures 45(21):5503-5520.

Wang, X., Wu, Z., (2010). Integrated High-Performance Thousand-Metre Scale Cable-Stayed Bridge With Hybrid FRP Cables. Composites: Part B 41:166-175.

Wang, Z.Y., Wang, Q.Y., (2015). Fatigue strength of CFRP strengthened welded joints with corrugated steel plates. Compos. Part B-Eng. 72:30-39.